

Evaluating the Impact of Climate Change on Future Bioretention Performance Across the Contiguous United States

Matthew Weathers[1*], Jon M. Hathaway[1], R. Andrew Tirpak[2], and Anahita Khojandi[3]

[1] Department of Civil and Environmental Engineering, University of Tennessee, Knoxville, TN, USA
[2] Department of Food, Agricultural, and Biological Engineering, The Ohio State University, Columbus, OH, USA
[3] Department of Industrial and Systems Engineering, University of Tennessee, Knoxville, TN, USA
*Corresponding author: mweath11@vols.utk.edu

Abstract

In light of shifting precipitation patterns induced by climate change, communities are seeking to build resiliency in urban drainage systems through interventions such as green stormwater infrastructure (GSI). Bioretention cells are one of the most commonly implemented forms of GSI for their ability to reduce peak discharge, retain runoff, and filter pollutants. However, they may be at risk of reduced function in the future due to deviations from historic precipitation frequency and intensity patterns which are essential to their design. Further, changes in future function are likely to vary regionally as the magnitude of future climate changes will differ across the globe. To explore the range of impacts to future bioretention function, an ensemble of 10 regional climate models at 17 locations across the contiguous United States were evaluated to provide the widest range of potential future outcomes using a probabilistic approach to capture the uncertain nature of climate change. Bioretention cells were modeled using USEPA's Storm Water Management Model (SWMM) to compare existing and future performance under a range of climate change projections. Median annual rainfall and 99th percentile rainfall event depths and intensities were projected to increase across all 17 locations while antecedent dry period (i.e., the time between consecutive rain events) was projected to increase for 11 locations. Correspondingly, bioretention cell hydrologic performance decreased across all 17 locations under future scenarios: relative to performance under current climate conditions, annual volumes of infiltration decreased between 4.0-24.0% across all 17 locations while overflow increased between 0.4-19.6% for 15 locations. Results suggest that bioretention cells in the southern United States are at significant risk of reduced function in the future while those in the Midwest and Northeast are at moderate risk. Bioretention cells in the Northwest/West performed the best under future climate scenarios; that is, they showed similar function in the future to that of the present. Findings demonstrate that most, if not all, bioretention cells across the contiguous United States will require some degree of modification to maintain existing function under future conditions.

Keywords: Green infrastructure; urban hydrology; climate change; stormwater; SWMM

1.0 Introduction

The increased likelihood of extreme weather events (e.g., frequent floods, drought conditions, record-breaking temperatures) associated with anthropogenic activities has been well documented (Masson-Delmotte et al., 2018). For example, Bishop et al. (2019) found a 40% increase in fall precipitation for the period 1895-2018 in the southeastern United States, with nearly all of the added precipitation occurring with an increased intensity. Similarly, using datasets from 182 stations across the contiguous United States, Karl and Knight (1998) noted a 10% increase in precipitation over the twentieth century primarily due to heavy and extreme precipitation events with 53% of the added precipitation attributable to the upper 10% of the precipitation distribution. According to Prudhomme et al. (2014), if anthropogenic activities and emissions continue to increase at the current rate, then Southern Europe, the Middle East, the Southeast United States, Chile, and South West Australia are at significant risk of experiencing droughts and water security issues by the year 2100.

At the same time, the rapid urbanization across the planet has led to a greater percentage of urban areas becoming covered by impervious surfaces that prevent soil infiltration (Shuster et al., 2005). These shifts result in increased runoff and flooding (Du et al., 2012), increased nonpoint source pollution (O'Driscoll et al., 2010), and a suite of degraded conditions in receiving waters referred to as the urban stream syndrome (Walsh et al., 2005). The combination of climate change and rapid urbanization poses serious risks for public health and safety. Zhang et al. (2018) showed that the extreme flooding caused by Hurricane Harvey in August 2017 was intensified due to both anthropogenic-induced climate change and the effects of increased urbanization in Houston, Texas, USA. Similarly, Yang et al. (2021) found that the extreme rainfall and flooding in Western Europe during July 2021 was exacerbated due to urbanization and urban-induced rainfall anomalies. Such extreme precipitation events have provoked efforts to mitigate the worsening effects of climate change.

Stormwater management systems, which are typically broken into two categories, gray and green, represent critical infrastructure components which are directly threatened by climate change. Green stormwater infrastructure (GSI) is increasingly utilized in urban areas to assist and supplant existing gray stormwater infrastructure and enhance the resilience of urban drainage networks to climate change (Eckart et al., 2017; Huang et al., 2018). One of the most commonly implemented and studied types of GSI is the bioretention cell, which consists of layers of gravel, soil, sand, organic matter, and plants (TDEC, 2014). Bioretention cells provide effective removal of total suspended solids (TSS) and pollutants (e.g., TN, TP) (Davis et al., 2001) while reducing runoff volume and peak discharge (Dietz, 2007; Winston et al., 2016; Davis 2008).

Despite research showing the benefits of bioretention under existing climate regimes, the use of these systems for climate change mitigation and environmental sustainability is underpinned by their ability to function under future climate scenarios, which is effectively the climate resiliency of bioretention (Hettiarachchi et al., 2022b). Historically, hydrologic engineering designs (including bioretention) have relied on the stationarity of rainfall patterns. However, recent research has shown that this can no longer be assumed with a shift towards increasingly frequent and more intense storm events (Milly et al., 2008; Pryor et al., 2009; Cook et al., 2020; Rosenberg et al., 2010). Wasko and Sharma (2015) and Hettiarachchi et al. (2018) also found that warming temperatures associated with future climate regimes could increase the variability of storm temporal patterns, further stressing stormwater infrastructure. Thus, a number of studies have begun to use projections from regional climate models (RCMs) and general circulation models (GCMs) to understand potential shifts in hydrologic processes and the resulting effects on critical infrastructure (Arnbjerg-Nielsen, 2012; Cook et al., 2019; Sarkar et al., 2018).

Recent studies have implemented a similar approach to investigate the future function of bioretention cells under climate change. Hathaway et al. (2014) evaluated future performance of four bioretention cells in Rocky Mountain and Nashville, North Carolina, USA, using one RCM and two representative concentration pathways (RCPs). Comparing historic (2001-2004) with projected (2055-2058) performance, results showed that the frequency and volume of overflow could increase significantly for projected scenarios, requiring an additional storage of between 9 and 31cm to limit increases in annual overflow under future conditions. Zhang et al. (2019) evaluated a range of design configurations for a bioretention cell in Melbourne, Australia, using eight GCMs and one RCP. Comparing historic (1995-2004) with projected (2040-2049) performance, results suggested that larger bioretention cells should be prioritized due to the variability of future GCM scenarios. Similarly, Tirpak et al. (2021) evaluated a range of design configurations for a bioretention cell in Knoxville, Tennessee, USA, using 10 RCMs, two RCPs, and three underlying soil types with infiltration rates ranging from 0.13 cm/hr to 2.5 cm/hr. Comparing historic (2010-2014) with projected (2040-2044) performance, results showed that even the most significant retrofit configurations led to overflow increases in 67.4% to 71.1% of simulations – with underlying soil type having minimal effect on overflow – indicating the significant impact of shifting precipitation patterns. Wang et al. (2019a) performed a similar study by evaluating a range of bioretention cell surface areas in Guangzhou, China, using 11 GCMs, four RCPs, and six design storms. Results showed that future bioretention cells could maintain existing function for small, short-duration storms by increasing surface area, but function will diminish as storm size and duration increase regardless of increases in surface area.

Highlighting regional differences in future climate, Winston (2016) evaluated future performance of bioretention cells located 25 km apart in northeast Ohio, USA, using one GCM and two RCPs. Comparing historic (2001-2004) with projected (2055-2059) performance, results showed that bioretention cells mitigated 5-9% less runoff in one location while mitigating 4-6% more runoff in the other location.

As such, while some research has been performed investigating the performance of a single bioretention cell under future precipitation patterns, almost no research has been performed comparing multiple locations across the United States or the globe, for that matter. There is a need to explore the geographic variability in the effects of climate change on existing GSI to better understand the regional adaptations that may be required to prepare for these impacts. To address this knowledge gap, this study explores changes in bioretention performance under future climate change scenarios in 17 locations across the United States selected based off their unique hydrologic region. Ten Regional Climate Models (RCMs) were selected from the North American Coordinated Regional Downscaling Experiment (NA-CORDEX) to provide a wide range of potential future precipitation outcomes at each location (Mearns et al., 2017). The objective of this effort was to identify shifts in bioretention performance from historical to future conditions and to better understand the geographic variability of impacts to future performance. Results from this work can be used to identify locations where bioretention cells may be most adversely affected by climate change, and thus may require modifications to ensure their desired performance persists in the future.

2.0 Data Collection and Methodology

2.1 Data Collection

Observed climate data were acquired from the National Oceanic and Atmospheric Administration (NOAA) National Centers for Environmental Information (NCEI) data archive to allow for bias-correction of climate model outputs and characterization of historical bioretention function (NOAA, 2016). Simulated historic and future climate data were acquired from the North American Coordinated Regional Downscaling Experiment (NA-CORDEX) data archive (Mearns et al., 2017). Climate data were acquired for 17 locations across the US (Table 1), which were selected based on their unique hydrologic region defined by the Bukovsky climate map (Bukovsky et al., 2019). The Bukovsky climate map groups regions by hydrologic similarity, accounting for average temperature and rainfall as well as seasonal occurrences such as the North American monsoon (Bukovsky, 2011). Using the same cities as Cook et al. (2019), each climate region in the contiguous US was represented by at least one city in the analysis.

Table 1. Characteristics of US cities used in this study

City	State	Bukovsky Region	Latitude[a]	Longitude[a]	NOAA NCEI Station Name
Amarillo	TX	C. Plains	35.2220°	-101.8313°	AMARILLO AIRPORT TX US
Boise	ID	Great Basin	43.6150°	-116.2023°	BOISE AIR TERMINAL ID US
Boston	MA	North Atlantic	42.3601°	-71.0589°	BOSTON MA US
Boulder	CO	S. Rockies	40.0169°	-105.2796°	BOULDER 2 CO US
Charlotte	NC	Mid Atlantic	35.2271°	-80.8431°	CHARLOTTE DOUGLAS AIRPORT NC US
Chicago	IL	Great Lakes	41.8832°	-87.6324°	CHICAGO OHARE INTERNATIONAL AIRPORT IL US
El Paso	TX	Mezquital	31.7619°	-106.4850°	EL PASO INTERNATIONAL AIRPORT TX US
Fargo	ND	N. Plains	46.8772°	-96.7898°	FARGO HECTOR INTERNATIONAL AIRPORT ND US
Memphis	TN	Deep South	35.1495°	-90.0490°	MEMPHIS INTERNATIONAL AIRPORT TN US
Missoula	MT	N. Rockies	46.8721°	-113.9940°	MISSOULA INTERNATIONAL AIRPORT MT US
New Orleans	LA	Southeast	29.9511°	-90.0715°	NEW ORLEANS AIRPORT LA US
Phoenix	AZ	Southwest	33.4484°	-112.0740°	PHOENIX AIRPORT AZ US
Pittsburgh	PA	Appalachia	40.4406°	-79.9959°	PITTSBURGH ASOS PA US
Portland	OR	Pacific NW	45.5122°	-122.6587°	PORTLAND INTERNATIONAL AIRPORT OR US
San Antonio	TX	S. Plains	29.4241°	-98.4936°	SAN ANTONIO INTERNATIONAL AIRPORT TX US
San Jose	CA	Pacific SW	37.3348°	-121.8881°	SAN JOSE CA US
St. Louis	MO	Prairie	38.6270°	-90.1994°	ST LOUIS LAMBERT INTERNATIONAL AIRPORT MO US

[a]Values provided by latlong.net

Observed daily temperature (maximum and minimum) and hourly precipitation data from January 1, 1999, to December 31, 2013, were gathered from the NOAA NCEI archive for all 17 locations (NOAA, 2016). The 15-year period was selected to fully capture the year-to-year variability of recent precipitation and temperature patterns, subject to data availability. The 17 NOAA NCEI stations shown in Table 1 were selected based off the availability of continuous climate data for the time range specified and their proximity to the selected cities.

Covering the majority of North America, the NA-CORDEX data archive provides simulated climate data from a range of RCMs produced using boundary conditions from GCMs in the Coupled Model Intercomparison Project Phase 5 (CMIP5) (Mearns et al., 2017). As recommended by Bukovsky and Mearns (2020), all ten NA-CORDEX climate models with available hourly precipitation projections were used for this study to provide the most comprehensive range of potential future outcomes (Table 2). Due to the limited availability of hourly precipitation projections in the archive, only one RCP4.5 scenario (representing moderate population growth, moderate climate policy, and eventual decline and stabilization of anthropogenic emissions) was evaluated while nine RCP8.5 scenarios (representing high population growth, no climate policy, and rapid increase in anthropogenic emissions) were evaluated (van Vuuren et al., 2011). Both historic simulated climate data from January 1, 1999, to December 31, 2013, and future simulated climate data from January 1, 2035, to December 31, 2049, were acquired to allow for bias-correction and SWMM modeling.

Table 2. Characteristics of NA-CORDEX climate models used in this study[a]

Model	RCP	GCM	RCM	Spatial Resolution
1	4.5	CanESM2	CanRCM4	50km
2	8.5	CanESM2	CanRCM4	50km
3	8.5	GFDL-ESM2M	WRF	25km
4	8.5	GFDL-ESM2M	WRF	50km
5	8.5	HadGEM2-ES	WRF	25km

6	8.5	HadGEM2-ES	WRF	50km
7	8.5	MPI-ESM-LR	RegCM4	25km
8	8.5	MPI-ESM-LR	RegCM4	50km
9	8.5	MPI-ESM-LR	WRF	25km
10	8.5	MPI-ESM-LR	WRF	50km

[a]NA-CORDEX data provided by Mearns et al. (2017)

2.2 Bias Correction

Systematic bias was corrected in climate model outputs following data acquisition. Due to bias introduced during model formulation and the downscaling process, bias-correction procedures must be applied to more accurately align modeled climate data with observed climate data (Rosenberg et al., 2010). Stephens et al. (2010) compared five different weather prediction, climate, and global cloud "resolving" models and found that all models overproduced precipitation frequency by a factor of two while underproducing precipitation intensity compared with observed precipitation data. Bias-correction is, therefore, required prior to SWMM modeling to ensure that RCM inputs provide statistically accurate distributions.

The kernel density distribution mapping (KDDM) bias-correction procedure was selected due to its accuracy, ease of implementation (McGinnis and Mearns, 2016; Tirpak et al., 2021), and overall performance compared with other bias-correction procedures (McGinnis et al., 2015). KDDM applies a set of bias-correction steps to scale the distribution of climate projections to match that of observed climate data. Due to the frequent over-prediction of low intensity precipitation (Stephens et al., 2010), the excess "drizzle" was first removed from projected rainfall by setting hourly precipitation volumes below a minimum threshold to zero in order to match the wet/dry ratio of timesteps in the observed precipitation data (McGinnis and Mearns, 2016).

Following this "dedrizzling" step, nonparametric estimates of the underlying probability density functions (PDFs), similar to smooth, non-discrete histograms, were produced for the observed and simulated precipitation datasets. The resulting PDFs were integrated using the trapezoidal rule to approximate cumulative distribution functions (CDFs). A transfer function was then created by fitting a spline between the corresponding quantiles for the inverse CDF of the observed precipitation data and the forward CDF of the simulated precipitation data (McGinnis et al., 2015). Lastly, the transfer function was applied to both the historic and future simulated precipitation data, yielding bias-corrected projections of future rainfall. KDDM bias-correction of the simulated temperature data followed the same steps as the precipitation bias-correction, with the exception of the "dedrizzling" step, and was performed on a monthly basis to account for seasonal variability (McGinnis et al., 2015). Bias-correction via KDDM was applied to all projections of precipitation and temperature records for each of the 17 cities of interest.

In a single instance, extreme values were removed from observed climate data to improve bias-correction. The September 2013 floods in Boulder, CO, resulted in 231mm of rainfall recorded on September 12 (NOAA, 2016), nearly doubling the previous daily record of 122mm (Hamill, 2014). According to the NOAA National Weather Service Precipitation Frequency Data Server (NOAA, 2017), the 24-hr, 1000-year precipitation depth for Boulder, CO, is 207mm, 24mm less than the rainfall on September 12, 2013, further illustrating the rarity of the precipitation event. Cook (2018) reported that extreme values in observed data used to bias-correct simulated data may lead to inaccurate annual maximum values obtained through KDDM bias-correction. As such, observed hourly precipitation data from September 9, 2013, through September 16, 2013, for Boulder, CO, were replaced with the median precipitation depth for that time period using the previous 14-year record. Removal of these extreme values resulted in bias-corrected simulated precipitation data that more accurately reflected the distribution of the observed precipitation data.

KDDM bias-correction of the simulated hourly precipitation and daily temperature data was performed using the R package “climod” (McGinnis, 2018; R Core Team, 2020). Similar to analysis in Tirpak et al. (2021), the Wilcoxon rank sum test was used to confirm the statistical similarities between the distributions of observed and bias-corrected climate data for all 10 models across all 17 locations. Based on these results, the bias-corrected future climate data was determined to be suitable for subsequent SWMM modeling. Following bias-correction, an implausibly high precipitation depth was noted in the bias-corrected future dataset in El Paso using Model 6 (9615mm in 4 hours). The precipitation amount was removed and set to 0mm for the 4-hour time period, subsequently producing future precipitation statistics in line with the other nine models.

2.3 SWMM Modeling

The USEPA Storm Water Management Model (SWMM) version 5.1 was used in this study for its ability to provide dynamic rainfall-runoff relationships for long-term simulations (Gironás et al., 2009) and capacity to directly model bioretention cells using the LID Control Editor (Rossman, 2015). The SWMM model was designed to simulate a hypothetical 0.4-hectare (4,000 m^2) subcatchment, a bioretention cell, a rain gage, and an outlet. Detailed design characteristics for the subcatchment are shown in Table 3. The subcatchment was designed with 100% impervious cover to represent a common impervious surface in a city such as a parking lot. A Manning’s n value of 0.01 was selected for the impervious surface to account for the hydraulic efficiency of the subcatchment (Arcement and Schneider, 1989). All runoff from the subcatchment was routed directly to the bioretention cell.

Table 3. Subcatchment design characteristics

Parameter	Description	Value	Unit
Area	Area of subcatchment	0.4	hectare

Width	Width of overland flow path for sheet flow runoff	76.2	m
% Slope	Average surface slope	1	%
% Imperv	Percent impervious area	100	%
N-Imperv	Manning's n for overland flow across impervious area	0.01	-
Dstore-Imperv	Depression storage depth for impervious area	0	cm
%Zero-Imperv	Percent impervious area with zero depression storage	100	%
Subarea Routing	All runoff flows directly to outlet	OUTLET	-

While bioretention cell design guidelines vary by region, the same bioretention cell characteristics were used for all locations and models to ensure the only independent variable was climate (observed and bias-corrected future), allowing for relative changes in bioretention cell performance to be assessed. Bioretention cell design characteristics were based off the Baseline design scenario used by Tirpak et al. (2021), which incorporated design recommendations from the Tennessee Department of Conservation (TDEC, 2014), the Minnesota Stormwater Steering Committee (MSSC, 2006), the Knox County Tennessee Stormwater Management Manual (County, 2008), and the SWMM User's Manual version 5.1 (Rossman, 2015). This design was considered to be comparable to design standards in most locations (Aiona et al., 2020; LDEQ, 2010; MassDEP, 2008; NCDEQ, 2020; PWSA, 2022; SARA 2019).

Bioretention cell design characteristics used in the SWMM model are shown in Table 4. The surface area (534.2 m^2) and surface layer depth (15.2 cm) were sized to enable the bioretention cell to store the water quality storm event for the southeastern United States (Deletic, 1998; Pitt, 1999), which is typically the surface runoff generated from a 25.4-mm storm event. The soil layer was composed of a mixture of coarse sand, topsoil, and organic matter to filter pollutants while promoting flow through high hydraulic conductivity (5.1 cm/hr). The storage layer underlying the media was composed of ASTM #57 stone (nominal size of 4.75 to 25mm) with a high void ratio (0.4) to allow for water storage or seepage (1.3 cm/hr) into the native soil (ASTM, 2003). Lastly, the bottom of the underdrain pipe was placed at the top of the storage layer to allow the storage layer to completely fill prior to draining (Rossman, 2015).

Table 4. Bioretention cell design characteristics

Surface Parameter	Description	Value	Unit	Source
Berm Height	Max ponding depth above surface	15.2	cm	TDEC (2014)
Vegetation Volume Fraction	Fraction of volume filled with vegetation (ignored)	0	-	Rossman (2015)
Surface Roughness	Manning's n for overland flow (ignored)	0	-	Rossman (2015)
Surface Slope	Slope of surface (ignored)	0	%	Rossman (2015)
Soil Parameter	**Description**	**Value**	**Unit**	**Source**
Soil Thickness	Thickness of soil layer	61.0	cm	TDEC (2014)
Porosity	Pore space volume/total soil volume	0.44	-	MSSC (2006)
Field Capacity	Pore water volume/total soil volume (following drainage)	0.09	-	MSSC (2006)
Wilting Point	Pore water volume/total soil volume (for well-dried soil)	0.04	-	MSSC (2006)
Conductivity	Hydraulic conductivity of fully saturated soil	5.1	cm/hr	MSSC (2006)
Conductivity Slope	Slope of log(Conductivity) vs soil moisture content curve	50	-	Rossman (2015)
Suction Head	Soil capillary suction	10.2	cm	Brakensiek et al. (1981)
Storage Parameter	**Description**	**Value**	**Unit**	**Source**
Storage Thickness	Thickness of gravel layer	15.2	cm	County (2008)
Void Ratio	Void space volume/solid space volume	0.4	-	Miller (1978)
Seepage Rate	Rate of water seepage from storage layer into native soil	1.3	cm/hr	MSSC (2006)
Clogging Factor	Clogging parameter (ignored)	0	-	Rossman (2015)
Drain Parameter	**Description**	**Value**	**Unit**	**Source**
Flow Coefficient[a] (C)	Determines drain flow rate as function of hydraulic head	0.6	-	County (2008)
Flow Exponent[a] (n)	Determines drain flow rate as function of hydraulic head	0.5	-	County (2008)
Offset	Height of drain line above bottom of storage layer	15.2	cm	Miller (1978)

[a]Flow Coefficient and Flow Exponent are incorporated within $q = Ch^n$ where q is drain outflow rate (cm/hr) and h is height of saturated media above drain (cm) (Rossman, 2015).

The Rainfall/Runoff process model accounted for surface runoff from the subcatchment into the bioretention cell. The Green-Ampt infiltration model was used to represent soil infiltration using fundamental soil properties (i.e., initial soil moisture deficit, saturated hydraulic conductivity, and suction head at the wetting front) (Green and Ampt, 1911). Dynamic wave routing was used to solve the one-dimensional Saint-Venant equations and incorporate both the continuity and momentum equations (Rossman, 2015).

Data File inputs included observed hourly precipitation data (1999-2013) and bias-corrected future hourly precipitation data (2035-2049). The Climatology Editor was used to input External Climate Files containing observed daily temperature data (1999-2013) and bias-corrected future daily temperature data (2035-2049). The temperature files were used as the Source of Evaporation Rates in the Evaporation tab of the Climatology Editor, which estimates daily evaporation rates from daily temperature values using the Hargreaves method (Hargreaves and Samani, 1985; Rossman, 2015).

Following model setup, the model was run using the observed climate data (17 scenarios) from January 1, 1999, to December 31, 2013, and the bias-corrected future climate data (170 scenarios, which included 10 projections for each of the 17 cities used herein) from January 1, 2035, to December 31, 2049. Three bioretention cell outputs were compiled and assessed in this study (i.e., infiltration loss, underdrain outflow, and overflow). These three bioretention cell performance indices accounted for the majority of total inflow into the bioretention cell and provided quantitative measures for the efficacy of the bioretention cell. The sum of all three performance indices (i.e., infiltration loss, underdrain outflow, and overflow) over the entire simulation period (i.e., 15 years) is hereafter referred to as "cumulative volume."

Observed (1999-2013) and future (2035-2049) median average annual infiltration loss, underdrain outflow, and overflow volumes for all 17 locations were calculated for Figure 5. The values were calculated by dividing the median cumulative volume by the duration of the simulation period (i.e., 15 years) to yield an annual average. The sum of all three annualized performance indices (i.e., infiltration loss, underdrain outflow, and overflow) is hereafter referred to as "annual volume." Due to many locations having extremely low underdrain outflow or overflow under the observed precipitation dataset, relative comparisons between observed and future datasets have been made in Figure 5 using changes in the percent of total annual volume attributed to each hydrologic pathway as opposed to using percent change. Relative percent change between the observed and future datasets was calculated using Eq. 1.

$$relative\ \%\ change = future\ \% - observed\ \% \qquad \text{Eq. 1}$$

3.0 Results and Discussion

3.1 Precipitation Statistics

Due to the significant number of locations (17) and models (10), climate inputs were first analyzed to understand how precipitation varied based on both location and a given climate model. Comparison of observed and future datasets using both categories, location and model, provides context as to how assessments of climate change effects may yield variable results based on these factors. Bioretention cell performance was then assessed using three bioretention cell performance indices: infiltration loss, underdrain outflow, and overflow.

Due to the range of locations selected, it's important to first note the geographic and hydrologic variability of the United States. The 17 locations can be separated into the following five regions: the Northeast (Boston and Pittsburgh), the Midwest (Chicago, Fargo, and St. Louis), the Southeast (Charlotte, Memphis, and New Orleans), the Southwest (Amarillo, El Paso, Phoenix, and San Antonio), and the Northwest/West (Boise, Boulder, Portland, Missoula, and San Jose). The Northeast and Midwest are defined by humid continental climates with mild to hot summers and year-round precipitation; the Southeast is defined by a humid subtropical climate; the Southwest varies from cold semi-arid to hot desert climates; and the Northwest/West varies from cold semi-arid to humid continental to Mediterranean climates (Köppen, 1900). For example, in the eastern United States, Pittsburgh is between 550 and 950 km from Boston (776 km), Charlotte (584 km), Chicago (674 km), and St. Louis (898 km), and in the western United States, El Paso is also between 550 and 950 km from Amarillo (577 km), Boulder (923 km), Phoenix (555 km), and San Antonio (808 km). However, while the observed mean annual rainfall for these five eastern US locations ranges between 912 mm in Chicago and 1072 mm in Boston, the observed mean annual rainfall for these five western US locations ranges between 163 mm in Phoenix and 790 mm in San Antonio. Rainfall event depths also vary significantly by region, from 35 mm in Boise to 268 mm in New Orleans for observed 99.9th percentile rainfall event depths.

Figure 1 displays the percent change between the observed (1999-2013) and future (2035-2049) datasets for mean annual rainfall, mean annual rain events, mean annual rainy days, and mean drying period for the 17 locations. Rainy days were counted as any day in which rainfall depth was greater than 0.0 mm between 00:00 and 23:59. A minimum inter-event time (MIT) of 6-hours was used to separate rain events in the datasets (Chin et al., 2016; Palynchuk and Guo, 2007). Any period without rainfall for 6 hours or more was accounted for in the mean drying period (i.e., the time between consecutive rain events).

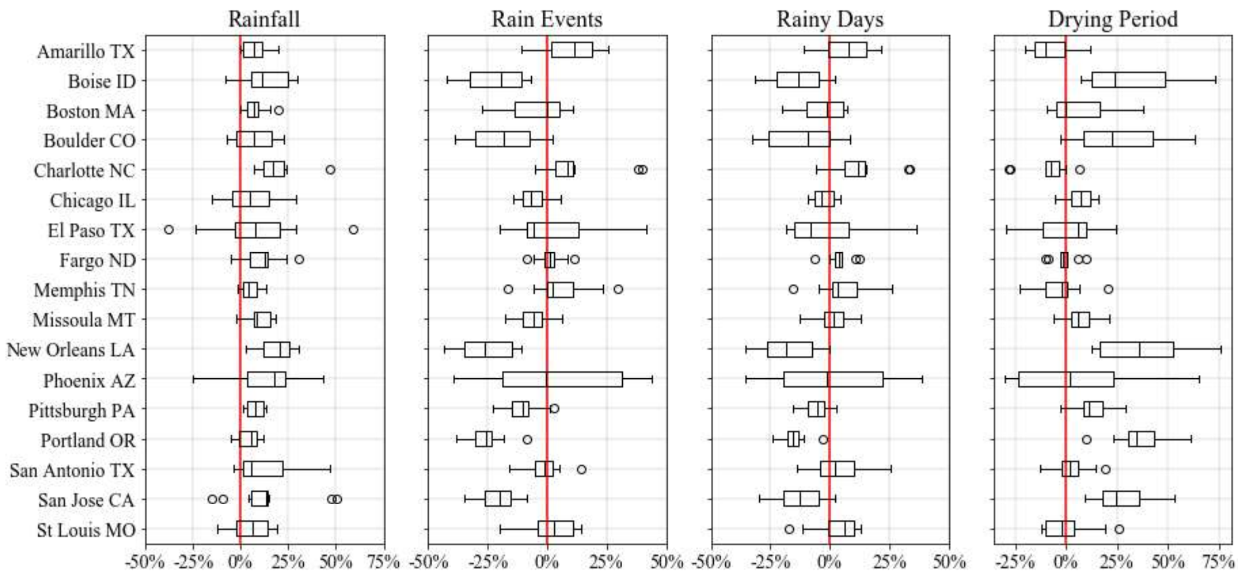

Fig. 1. Percent change between observed (1999-2013) and future (2035-2049) mean annual rainfall, mean annual rain events, mean annual rainy days, and mean drying period for the 17 locations. The solid red line marks zero percent change between observed and future values.

The boxplots for each location consist of the percent change between the observed and future datasets for all 10 models (i.e., 10 values per boxplot). Out of the 170 total future model-location combinations, annual rainfall increased in 135 combinations (79.4%), annual rain events decreased in 110 combinations (64.7%), annual rainy days decreased in 103 combinations (60.6%), and mean drying period increased in 107 combinations (62.9%). Median annual rainfall (shown as the solid black line inside each boxplot in Figure 1) increased for all 17 locations while the median number of annual rain events and rainy days decreased for nine locations with an additional three locations observing decreases in one of these two precipitation characteristics. Across all locations, mean annual rainfall depth increased by 9.9% (71mm) while mean annual rain events and rainy days decreased 6.2% (6.5 days) and 3.9% (3.7 days), respectively. The greatest percent change in mean annual rainfall (with an increase of 18.7%, corresponding to an additional 278mm of rainfall) occurred in New Orleans, while the lowest percent change occurred in Portland with an increase of 4.3% (38mm). These trends are consistent with the understanding that while the total amount of rainfall may be higher in many locations in the future, extreme rainfall will also increase in a significant number of locations due to climate change.

Coupled with an anticipated reduction in the number of rainfall events, climate change is expected to bring larger drying periods between storms (Zhang et al., 2019), further increasing the vulnerability of water scarce environments (Hettiarachchi et al., 2022a). Median drying period increased for 11 locations, but Portland was the only location where all 10 models projected increased annual dry days (i.e., a decrease in the average number of rainy days per year). The Northwest/West was the only region in which all locations (i.e., Boise, Boulder, Portland, Missoula, and San Jose) showed increases in median drying period, and excluding Missoula, account for four of the five largest percent increases in median drying period. As documented by Manka et al. (2016), the significant increase in median drying period in the Northwest/West could reduce the efficacy of biological processes present in bioretention cells resulting in nutrient export and the subsequent degradation of nearby waterways. Combining all locations, mean drying period increased by 10.5% (0.5 days) with the greatest percent change in mean drying period occurring in New Orleans (mean increase of 37.8% or 1.2 days), while no change occurred in St. Louis. Jhong and Tung (2018) also observed increases in the duration of future dry periods in Taiwan and suggested that occurrences of floods and droughts could occur more frequently due to the combination of increased precipitation event volumes and drying periods.

Figure 2 displays the percent change between observed (1999-2013) and future (2035-2049) precipitation depths for 50th, 90th, 99th, and 99.9th percentile rainfall event depths for the 17 locations. Out of the 170 total future model-location combinations, 50th percentile events increased in 62 combinations (36.5%), 90th percentile events increased in 118 combinations (69.4%), 99th percentile events increased in 165 combinations (97.1%), and 99.9th percentile events increased in 147 combinations (86.5%). While median 50th percentile events only increased in seven locations, the higher percentile events were consistently predicted to increase in size, with median 90th percentile events increasing in 12 locations, median 99th percentile events increasing in all 17 locations, and median 99.9th percentile events increasing in 16 locations. Rainfall intensities were projected to increase for an even greater number of locations and percentiles, with median 50th percentile rainfall intensities predicted to increase in 11 locations, median 90th percentile rainfall intensities predicted to increase in 15 locations, median 99th percentile rainfall intensities predicted to increase in all 17 locations, and median 99.9th percentile rainfall intensities predicted to increase in 15 locations.

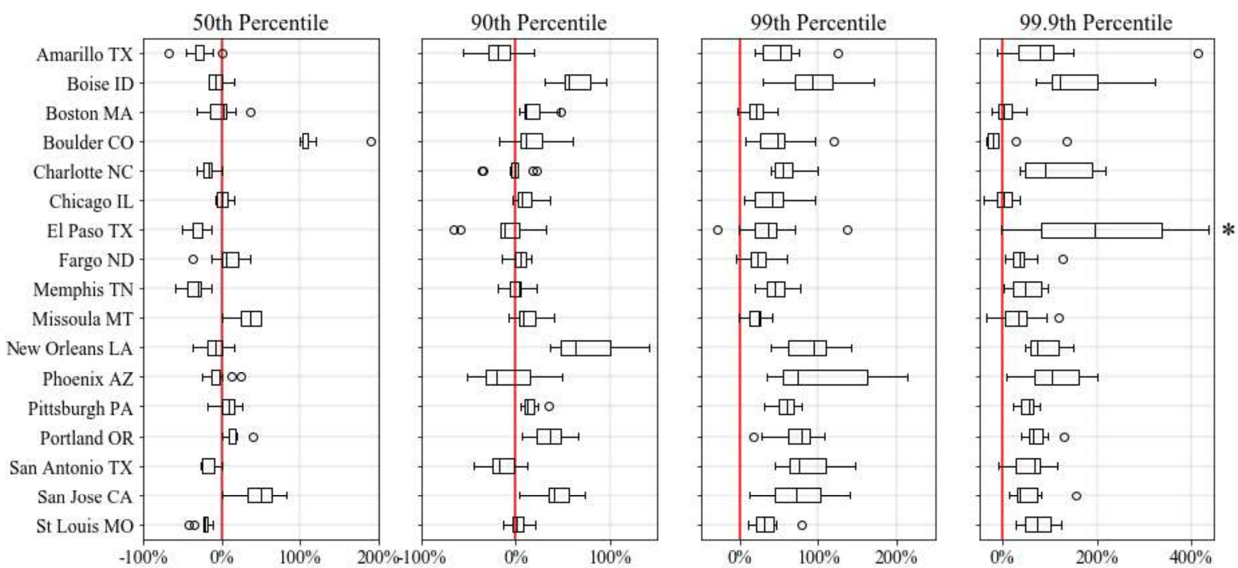

Fig. 2. Percent change between observed (1999-2013) and future (2035-2049) precipitation depths for 50th, 90th, 99th, and 99.9th percentile rainfall event depths for the 17 locations. The solid red line marks zero percent change between observed and future values.
*Note: An extreme outlier for 99.9th percentile events in El Paso is not shown in the figure (843%).

The trend in upper-percentile precipitation events and rainfall intensities ($\geq 90^{th}$) coupled with minimal changes to moderate precipitation events (i.e., 50^{th} percentile) supports findings in existing literature and again points to anticipated increases in severe rainfall in the future (Karl and Knight, 1998; Olsson et al., 2009). Since bioretention cells are most effective during small, lower-intensity precipitation events, the increase in the frequency of large, higher-intensity precipitation events is particularly concerning for future bioretention cell performance (Wang et al., 2018). The significant outliers in the 50^{th} (Boulder) and 99.9^{th} percentiles (El Paso) indicate that, as expected, climate change will not affect regional or even local precipitation equally. For example, the four locations (i.e., Boulder, Missoula, Portland, and San Jose) with the greatest increases in median 50^{th} percentile precipitation events occurred in the Northwest/West, while no location in the Southwest or Southeast showed an increase in median 50^{th} percentile precipitation events. Additionally, while those four locations (i.e., Boulder, Missoula, Portland, and San Jose) showed all 10 models projecting either increases or no change in 50^{th} percentile precipitation events, six locations (i.e., Amarillo, Charlotte, El Paso, Memphis, San Antonio, and St. Louis) showed all 10 models projecting either decreases or no change in 50^{th} percentile precipitation events – demonstrating the variability of future climate. Winston (2016) found similar variability in future precipitation when comparing locations only 25 km apart in northeast Ohio, USA. Similarly, Gao et al. (2012) showed substantial variability in climate change effects on extreme weather across the eastern United States.

3.2 Bioretention Cell Performance Statistics

Figure 3 displays the percent change between observed (1999-2013) and future (2035-2049) infiltration loss, underdrain outflow, and overflow from the modeled bioretention cell for all 17 locations. Due to a lack of overflow under the observed rainfall data (i.e., flow equal to zero), boxplots for Boise, Missoula, Phoenix, Portland, and San Jose are excluded from Figure 3 as percent change could not be calculated. Boise was the only location where both underdrain outflow and overflow did not occur under the observed rainfall data and also produced the lowest observed 99th and 99.9th percentile rainfall event depths out of all 17 locations, illustrating the relationship between bioretention performance and regional climate. While underdrain outflow and/or overflow box plots in Figure 3 could not be produced for these five locations (i.e., Boise, Missoula, Phoenix, Portland, and San Jose), underdrain outflow and overflow increased in all five locations under future scenarios, indicating even the best-performing bioretention cells may experience diminished performance under future climate change scenarios. These locations also produced five of the six lowest observed 99.9th percentile rainfall event depths and are the western-most out of all 17 locations, further illustrating the relationship between bioretention cell performance and regional climate. Additionally, overflow only occurred on two days (out of 15 years) under the observed rainfall data for El Paso. As such, percent change between observed and future overflow in El Paso appears more extreme in part due to the low number of overflow days for the observed dataset.

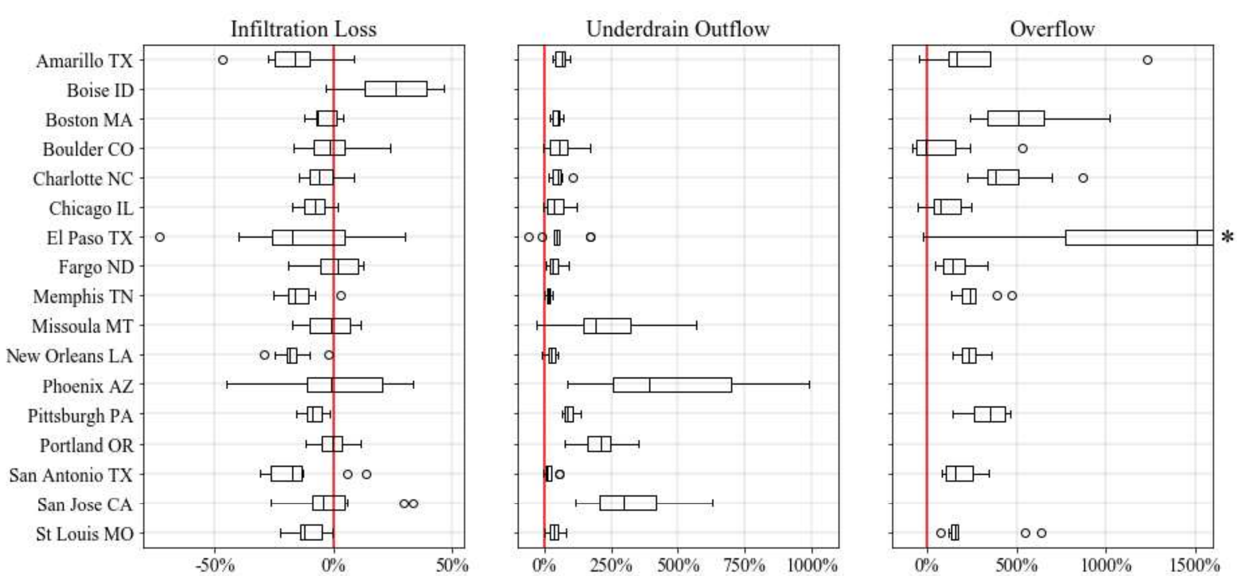

Fig. 3. Percent change between observed (1999-2013) and future (2035-2049) infiltration loss, underdrain outflow, and overflow from modeled bioretention cell for 17 locations. The solid red line marks zero percent change between observed and future values.
*Note: Second half of boxplot for El Paso is cut off from the figure (Q_3 = 2487%; Max = 5360%).

Excluding the two locations with increased median infiltration loss, Boise (25.9%) and Fargo (1.7%), percent change in median infiltration loss ranged from -0.2% (Portland) to -18.3% (New Orleans) in the remaining 15 locations. Conversely, excluding the one location with an observed underdrain outflow value of zero (Boise), percent change in median underdrain outflow increased between 9.7% (San Antonio) and 393.2% (Phoenix) in the remaining 16 locations. Finally, five locations had an observed overflow value of zero (i.e., percent change could not be calculated), while extreme outlier values were observed in two locations, namely Boulder (median decrease of 8.6%) and El Paso (median increase of 1510.4%). In the remaining 10 locations, the percent change in median overflow increased between 74.5% (Chicago) and 509.7% (Boston). Additionally, all locations in the Northeast (i.e., Boston and Pittsburgh) and Southeast (i.e., Charlotte, Memphis, and New Orleans) showed all 10 models projecting increases in overflow – with a minimum increase in overflow of 140% across the five locations. New Orleans, Pittsburgh, and St. Louis also showed all 10 models projecting decreases in median infiltration loss, indicating a high likelihood of diminished performance regardless of the future climate change scenario. The projected significant increase in overflow in 11 locations is most concerning from a public health and safety perspective due to the increased risk of flooding in urban areas (Hou et al., 2020; Olsson et al., 2009) and degradation of waterways caused by overflow predominantly bypassing treatment and quickly proceeding to nearby conveyances (Hathaway et al., 2014; Walsh et al., 2005).

Out of the 170 total future model-location combinations, overflow increased in 151 combinations (88.8%), underdrain outflow increased in 163 combinations (95.9%), and infiltration loss decreased in 121 combinations (71.2%). The increase in overflow and underdrain outflow combined with decreased infiltration loss indicate bioretention cells designed following current methods may be unable to accommodate the projected shift in precipitation patterns; specifically, surface infiltration rates may not be sufficient to avoid significant increases in overflow. While only a single underlying soil type (1.3 cm/hr) was evaluated in this study, results from Tirpak et al. (2021) indicate that underlying soil type has little effect on overflow. Thus, the primary benefits of bioretention cells (i.e., reducing peak runoff, groundwater recharge, and filtering pollutants) may be lessened under future climate change scenarios.

Decreased infiltration loss under increased rainfall volumes has been documented in previous literature (Tirpak et al., 2021), but the root cause has not been investigated. This is important as different design modifications may be needed depending on the primary contributors to decreased infiltration. This phenomenon is most likely due to the bioretention cell surface layer filling too quickly, overwhelming surface infiltration rates (and subsequent infiltration loss), and contributing to immediate overflow. If the surface layer is filling too quickly to enable surface infiltration, then the surface layer depth could be increased to hold a greater runoff volume, providing additional time for surface infiltration to occur (Tirpak et al., 2021). Real-time control (RTC) technologies could provide an additional option to decrease overflow and increase infiltration during moderate storm events through weather research and forecast (WRF) models and real-time sensors and controls (Klenzendorf et al., 2015), enabling bioretention cells to transition from passive stormwater management to active (Vijayaraghavan, et al., 2021). Compared to passive bioretention cells, Persaud et al. (2019) and Shen et al. (2020)

found that RTC technologies could provide both hydrologic and water quality improvements if retention time and storage are optimized for storm events. However, further research on the efficacy of RTC technologies for bioretention performance optimization is still required, and it's unlikely that RTC technologies could significantly reduce overflow during extreme storm events.

Figure 4 displays the percent change between observed (1999-2013) and future (2035-2049) mean yearly overflow days, 50th percentile daily overflow volume, 90th percentile daily overflow volume, and 99th percentile daily overflow volume. Overflow days were counted as any day in which overflow volume was greater than 0.0 m^3 between 00:00 and 23:59. Due to observed values of zero for overflow, Boise, Missoula, Phoenix, Portland, and San Jose are not shown in Figure 4 (i.e., percent change could not be calculated). Percent change in median yearly overflow days increased between 16.4% (New Orleans) and 347.5% (El Paso) for all 12 locations shown. Of the 12 locations shown in Figure 4, median number of annual rainy days also decreased in six locations (i.e., Boston, Boulder, Chicago, El Paso, New Orleans, and Pittsburgh) and, excluding Boulder and St. Louis, median ≥90th percentile rainfall intensities also increased for the 10 remaining locations, again indicating increases in rainfall magnitude and intensity when events do occur. A particularly compelling example of this trend is found in New Orleans, where a relatively low increase in median yearly overflow days was observed, yet a significant increase in median annual precipitation (18.7%) and 99th percentile rainfall intensities (21.3%) and decrease in median annual rainy days (19.5%) were observed – the largest percent changes in all three precipitation statistics – suggesting more intense events will make up a greater percentage of the storms that do occur. Given that bioretention cells are most effective during small, lower-intensity precipitation events, the efficacy of bioretention cells as a stormwater management practice in New Orleans may be questioned as large, higher-intensity precipitation events become the norm.

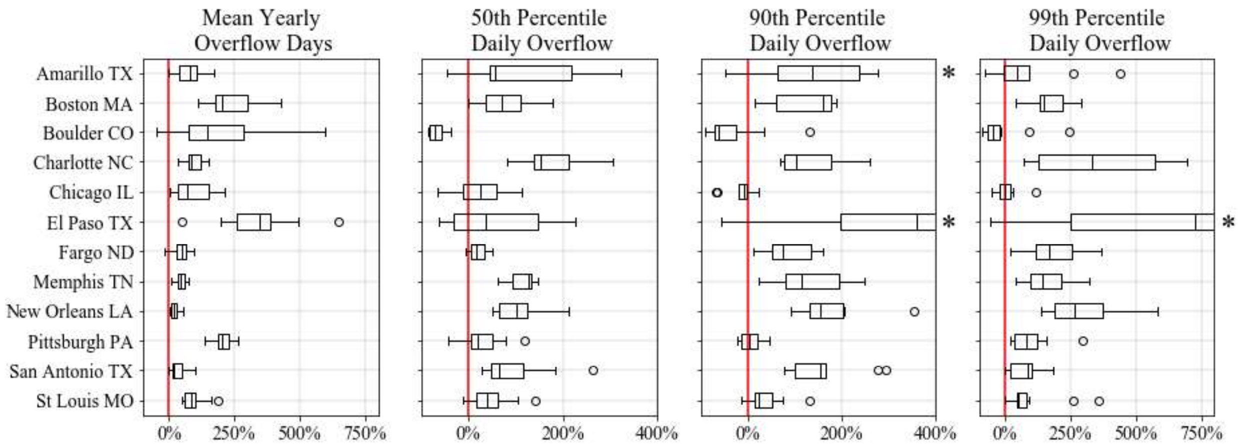

Fig. 4. Percent change between observed (1999-2013) and future (2035-2049) overflow characteristics for 12 locations. The solid red line marks zero percent change between observed and future values.
*Note: An outlier for Amarillo is cut off from the 90^{th} percentile figure (Max = 722%), and the second half of the boxplot for El Paso is cut off from the 90^{th} percentile figure (Q_3 = 701%; Max = 1158%) and 99^{th} percentile figure (Q_3=1220%; Max = 4436%).

Excluding Boulder and Chicago, median 50^{th}, 90^{th}, and 99^{th} percentile daily overflow increased for the 10 remaining locations shown in Figure 4. Excluding the Northwest/West, the consistent increase across all overflow percentiles indicates that government agencies, city planners, and stormwater engineers across the country should expect higher volumes to bypass treatment when overflow occurs from bioretention cells. Locations in the Southeast (i.e., Charlotte, Memphis, and New Orleans) face the greatest likelihood of higher overflow volumes. All three locations experienced ≥100% increases for all three (50^{th}, 90^{th}, and 99^{th}) median daily overflow percentiles, with all 10 climate models projecting increases in overflow compared with observed performance. Given the uniformity in predicted changes to a range of overflow volumes, adaptations to limit the environmental and public safety impacts of untreated bypass may be especially critical in these locations.

3.3 Regional Trends in Future Bioretention Cell Performance

Observed (1999-2013) and future (2035-2049) median average annual infiltration loss, underdrain outflow, and overflow volumes for all 17 locations are presented in Figure 5. Results indicate that bioretention cells in the southern United States (i.e., Southeast and Southwest) are most at risk of performance impacts under future climate change scenarios. The seven southern-most locations (i.e., Amarillo, Charlotte, El Paso, Memphis, New Orleans, Phoenix, and San Antonio) produced the highest relative percent increases in overflow, ranging from 7.0% to 19.6%. With the exception of Memphis, these locations also produced six of the highest relative percent decreases in infiltration loss, ranging from 15.3% to 24.0%. New Orleans and San Antonio also recorded the two highest relative increases in annual overflow volume, 2115.1 cu m/yr and 710.0 cu m/yr, respectively. Significant increases in overflow in the southern United States are consistent with extreme precipitation projections by Prein et al. (2017) and bioretention literature (Cook et al., 2019; Hathaway et al., 2014). The significant increases in overflow are a direct result of the frequent and intense rainfall in the southern United States, highlighting the potential limitations of current bioretention design strategies. Although GSI is likely to provide some resiliency to extreme precipitation, these results indicate there are limits in this resilience that can be exceeded.

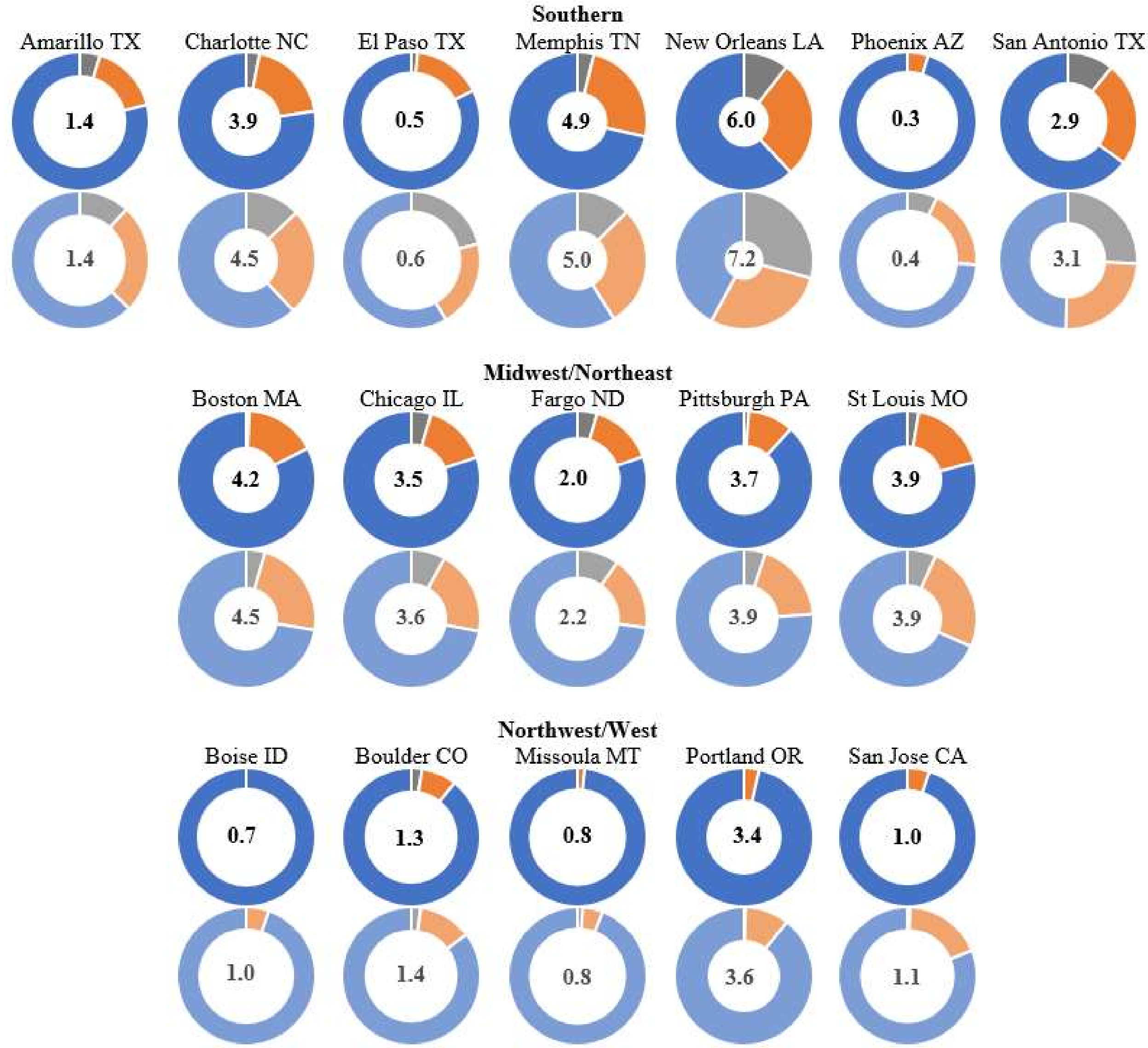

Fig. 5. Annual Volume (1000 cu m/yr) shown in the center of each donut chart is the sum of annual overflow, underdrain outflow, and infiltration loss. Observed (top) and future (bottom) overflow (grey), underdrain outflow (orange), and infiltration loss (blue) for all 17 locations. Donut hole size is inversely proportional to the annual volume.

Similarly, bioretention cells located in the Midwest and Northeast are still at risk of diminished performance under future climate change scenarios. Following the seven southern locations, the five locations in the Midwest and Northeast (i.e., Boston, Chicago, Fargo, Pittsburgh, and St. Louis) produced the next highest relative percent increases in overflow, ranging from 3.3% to 5.2%. The five Midwest and Northeast locations also recorded the 5th through 9th highest relative median increases in annual overflow volumes, ranging from 176.2 cu m/yr to 241.1 cu m/yr. Results are consistent with Cook et al. (2019) who found that overflow from bioretention cells in the Midwest and Northeast occurred at equal or greater magnitudes compared with other regions in the United States.

Bioretention cells in the Northwest/West have the best likelihood of being able to maintain existing function under future climate change scenarios, also consistent with previous findings (Cook et al. 2019). The five Northwest/West locations (i.e., Boise, Boulder, Missoula, Portland, and San Jose) produced the lowest relative percent changes in overflow, ranging from a decrease of 0.3% to an increase of 1.2%. These locations also recorded the lowest relative changes in annual overflow volume, ranging from a median decrease of 4.2 cu m/yr to an increase of 21.5 cu m/yr. The minimal effect on existing bioretention cell function indicates that stormwater infrastructure in the Northwest/West may require the least adaptation measures to maintain existing function under future climate conditions.

3.4 Implications to Bioretention Design and Adaptation Measures

While overflow and infiltration are expected to increase and decrease, respectively, under future climate conditions for many bioretention cells across the United States, modifications can be implemented to mitigate the effects of climate change to their performance. Tirpak et al. (2021) compared an ensemble of retrofit and design configurations for bioretention cells in east

Tennessee, and found varying degrees of success for three scenarios: 1) increasing the soil layer depth; 2) increasing the storage layer depth; 3) and increasing the bioretention cell surface area. Increasing the depth of the soil layer in the bioretention cell was shown to be a conservative yet effective method of increasing runoff volume retention (Tirpak et al., 2021). As such, increasing the depth of the soil layer for bioretention cells in regions where overflow is expected to modestly increase, such as the Northwest/West and parts of the Midwest, is a viable option requiring low investment, particularly for newly constructed cells. Increased soil layer depth can also increase pollutant removal and water storage (Hatt et al., 2009), which may mitigate plant stress in these systems in the drier climates projected for the Northwest/West.

Increasing the depth of the storage layer has been found to be an effective method of reducing overflow. Hathaway et al. (2014) found an increased storage layer depth from 9.0 to 31.0 cm would maintain existing function of bioretention cells in east North Carolina into the late 2050s. Similarly, Winston (2016) found that increasing storage layer depth from 5.0 to 17.0 cm would maintain existing function in northeast Ohio into the late 2050s. Increasing the storage layer depth has the potential to temporarily store a greater volume of runoff than increasing the soil layer depth but requires either deepening the bioretention cell or removing media from the soil layer, reducing the efficacy of pollutant removal. Further, substantial increases in surface storage depth may lead to public safety concerns due to the hazard posed by deeper ponding zones relative to nearby surfaces. However, increasing the storage layer depth has been shown to be more effective at reducing overflow than increasing the soil layer depth and should be considered if overflow reduction is a priority (Tirpak et al., 2021). Densely populated, highly urbanized locations with a need to mitigate projected increases in future overflow, such as

Chicago, Pittsburgh, or Boston, may greatly benefit from increased storage layer depths in bioretention cells.

The final viable option investigated by Tirpak et al. (2021) increased the surface area of bioretention cells relative to the subcatchment, which has been shown to be an effective method of reducing overflow and increasing infiltration due to increased soil and storage layer volumes (Wang et al., 2019b; Zhang et al. 2019). Increasing bioretention cell surface area requires the greatest investment of the three options and may not be viable in highly urbanized locations due to limited space or cost. However, locations in the southern United States, such as El Paso, San Antonio, Memphis, Charlotte, and New Orleans, may require significant investment in all stormwater infrastructure (both grey and green) to mitigate projected increases in overflow volumes. A location such as New Orleans, in particular, may need to incorporate bioretention cell modifications wherever possible to reduce the significant increases in overflow volumes projected under future climate conditions.

Given the geographic and hydrologic variability of the US locations selected for this study, the bioretention cell modifications suggested could be applied to a range of cities globally. Locations projected to experience fewer rainfall events and longer dry periods, such as Melbourne, Australia (Zhang et al., 2019), could increase soil layer depths of bioretention cells to mitigate plant stress and improve pollutant removal. High-density locations with humid continental climates similar to Boston and Pittsburgh, such as Vienna, Austria (Strauss et al., 2012), may benefit from increasing the storage layer depth in bioretention cells depending on the severity of future climate conditions. Subtropical locations similar to New Orleans and Charlotte, such as Guangzhou, China (Wang et al., 2019a), will likely require considerable bioretention cell modifications wherever possible.

4.0 Conclusions

Bioretention performance under future climate change projections was evaluated for 17 cities across the contiguous United States using SWMM version 5.1. Median annual rainfall increased across all 17 locations in future scenarios. A majority of locations also experienced a decreased median number of rainy days and rain events while median drying period increased. Precipitation events were projected to become more severe for upper-percentile events ($\geq 90^{th}$) while 50^{th} percentile events were projected to change minimally for all locations except for Boulder. Future precipitation events were projected, therefore, to become less frequent but more severe. However, findings clearly indicate that while precipitation event severity is expected to increase on average across the United States the shift in precipitation patterns will vary significantly by location.

As a result of shifting precipitation patterns, future bioretention cell performance was impacted by changing climates across all locations. Results demonstrated that bioretention cells in the southern United States have the greatest likelihood of diminished future function, followed by cells in the Midwest and Northeast. Due to the magnitude of change projected for the Northwest/West, bioretention cells in those regions may only require minor investments in retrofits or design modifications to maintain future performance.

Increased annual overflow, which poses significant environmental and health risks to urban communities, projected for the Midwest, Northeast, and southern United States, may elevate the importance of design modifications (e.g., increasing surface storage layer volumes) to offset these risks. Projected decreases in infiltration from bioretention cells, especially notable in the southern United States, presents additional challenge for city planners and stormwater engineers. If bioretention cells are no longer able to promote infiltration into native soils and filter pollutants from runoff, then their benefit as a stormwater control measure will be substantially reduced. Further, these outcomes suggest that while bioretention following current design strategies may continue to provide some runoff mitigation, shifting precipitation patterns, including more intense rain events, reveal limitations in their ability to maintain desired performance under future climate conditions.

Future studies should consider a wider range of climate models, emissions scenarios, and bioretention cell configurations to provide an even more robust assessment of future impacts to performance. Additionally, while a range of climate models and locations were evaluated in this study, a single bioretention cell configuration was used for all simulations. Studies which consider multiple bioretention cell configurations would provide insight on the significance of design modifications beyond current standards for a range of locations to maintain existing function under future climate scenarios.

Acknowledgements

This work was supported by the National Science Foundation [grant number 1634975]. The authors would like to thank Dr. Seth McGinnis and Dr. Lauren Cook for their assistance with the bias correction procedure and Dr. Sean Arms for his assistance in acquiring the climate projections used in this research.

References

Aiona, A., Coker, A., Dunlap, I., Simpson, A., Stevens, H., 2020. City of Portland Stormwater Management Manual. Compiled by Bureau of Environmental Services, Portland, OR.

American Society for Testing and Materials (ASTM), 2003. C 33 Standard Specification for Concrete Aggregates. American Society for Testing and Materials, Philadelphia, PA.

Arcement, G. J., Schneider, V. R., 1989. Guide for selecting Manning's roughness coefficients for natural channels and flood plains. US Geology Survey, Denver, CO.

Arnbjerg-Nielsen, K., 2012. Quantification of climate change effects on extreme precipitation used for high resolution hydrologic design. *Urban Water J.* 9(2): 57-65. https://doi.org/10.1080/1573062X.2011.630091.

Ault, T. R., Cole, J. E., Overpeck, J. T., Pederson, G. T., Meko, D. M., 2014. Assessing the Risk of Persistent Drought Using Climate Model Simulations and Paleoclimate Data. *J. Clim.* 27(20): 7529-7549. https://doi.org/10.1175/JCLI-D-12-00282.1.

Bishop, D. A., Williams, A. P., Seager, R., 2019. Increased Fall Precipitation in the Southeastern United States Driven by Higher- Intensity, Frontal Precipitation. *Geophys. Res. Lett.* 46(14): 8300-8309. https://doi.org/10.1029/2019GL083177.

Brakensiek, D. L., Engleman, R. L., Rawls, W. J., 1981. Variation within Texture Classes of Soil Water Parameters. Transactions of the ASAE 24(2): 0335-0339. https://dx.doi.org/10.13031/2013.34253.

Bukovsky, M. S., 2011. Masks for the Bukovsky regionalization of North America. Regional Integrated Sciences Collective, Institute for Mathematics Applied to Geosciences, National Center for Atmospheric Research. Accessed March 2, 2021. http://www.narccap.ucar.edu/contrib/bukovsky/.

Bukovsky, M. S., Thompson, J. A., Mearns, L. O., 2019. Weighting a regional climate model ensemble: Does it make a difference? Can it make a difference? *Clim. Res.* 77(1): 23-43. https://doi.org/10.3354/cr01541.

Bukovsky, M. S., Mearns, L. O., 2020. Regional climate change projections from NA-CORDEX and their relation to climate sensitivity. *Clim. Change* 162(2): 645-665. https://doi.org/10.1007/s10584-020-02835-x.

Chin, R. J., Lai, S. H., Chang, K. B., Jaafar, W. Z. W., Othman, F., 2016. Relationship between minimum inter-event time and the number of rainfall events in Peninsular Malaysia. *Weather* 71(9): 213-218. https://doi.org/10.1002/wea.2766.

Cook, L. M., 2018. Using climate change projections to increase the resilience of stormwater infrastructure designs under uncertainty. Doctoral dissertation, Pittsburgh, PA: Carnegie Mellon Univ.

Cook, L. M., VanBriesen, J. M., Samaras, C., 2019. Using rainfall measures to evaluate hydrologic performance of green infrastructure systems under climate change. *Sustainable Resilient Infrastruct.* 1-25. https://doi.org/10.1080/23789689.2019.1681819.

Cook, L. M., McGinnis, S., Samaras, C., 2020. The effect of modeling choices on updating intensity-duration-frequency curves and stormwater infrastructure designs for climate change. *Clim. Change* 159(2): 289-308. https://doi.org/10.1007/s10584-019-02649-6.

County, K., 2008. Knox County Tennessee stormwater management manual. Compiled by AMEC Earth & Environmental Inc, Knoxville, TN.

Davis, A. P., 2008., Field Performance of Bioretention: Hydrology Impacts. *J. Hydrol. Eng.* 13(2): 90-95. https://doi.org/10.1061/(ASCE)1084-0699(2008)13:2(90).

Davis, A. P., Shokouhian, M., Sharma, H., Minami, C., 2001. Laboratory Study of Biological Retention for Urban Stormwater Management. *Water Environ. Res.* 73(1): 5-14. https://doi.org/10.2175/106143001X138624.

Deletic, A., 1998. The first flush load of urban surface runoff. *Water Res.* 32(8): 2462-2470. https://doi.org/10.1016/S0043-1354(97)00470-3.

Dietz, M. E., 2007. Low Impact Development Practices: A Review of Current Research and Recommendations for Future Directions. *Water Air Soil Pollut.* 186(1-4): 351-363. https://doi.org/10.1007/s11270-007-9484-z.

Du, J., Qian, L., Rui, H., Zuo, T., Zheng, D., Xu, Y., Xu, C. Y., 2012. Assessing the effects of urbanization on annual runoff and flood events using an integrated hydrological modeling system for Qinhuai River basin, China. *J. Hydrol.* 464-465: 127-139. https://doi.org/10.1016/j.jhydrol.2012.06.057.

Dupont, B., Allen, D. L., 1999. Revision of the Rainfall-intensity Duration Curves for the commonwealth of Kentucky.

Eckart, K., McPhee, Z., Bolisetti, T., 2017. Performance and implementation of low impact development – A review. *Sci. Total Environ.* 607-608: 413-432. https://dx.doi.org/10.1016/j.scitotenv.2017.06.254.

Gao, Y., Fu, J. S., Drake, J. B., Liu, Y., Lamarque, J. F., 2012. Projected changes of extreme weather events in the eastern United States based on a high resolution climate modeling system. *Environ. Res. Lett.* 7(4): 044025. https://dx.doi.org/10.1088/1748-9326/7/4/044025.

Gironás, J., Roesner, L. A., Davis, J., 2009. Storm Water Management Model Applications Manual. US Environmental Protection Agency, EPA: Washington, DC, US.

Green, W. H., Ampt, G. A., 1911. Studies on Soil Phyics. *J. Agric. Sci.* 4(1): 1-24. https://dx.doi.org/10.1017/s0021859600001441.

Hamill, T. M., 2014. Performance of Operational Model Precipitation Forecast Guidance during the 2013 Colorado Front-Range Floods. *Mon. Weather Rev.* 142(8): 2609-2618. https://dx.doi.org/10.1175/mwr-d-14-00007.1.

Hargreaves, G. H., Samani, Z. A., 1985. Reference Crop Evapotranspiration from Temperature. *Appl. Eng. Agric.* 1(2): 96-99. https://doi.org/10.13031/2013.26773.

Hathaway, J. M., Brown, R. A., Fu, J. S., Hunt, W. F., 2014. Bioretention function under climate change scenarios in North Carolina, USA. *J. Hydrol.* 519: 503-511. https://doi.org/10.1016/j.jhydrol.2014.07.037.

Hatt, B. E., Fletcher, T. D., Deletic, A., 2009. Hydrologic and pollutant removal performance of stormwater biofiltration systems at the field scale. *J. Hydrol.* 365(3): 310-321. https://doi.org/10.1016/j.jhydrol.2008.12.001.

Hettiarachchi, S., Wasko, C., Sharma, A., 2018. Increase in flood risk resulting from climate change in a developed urban watershed–the role of storm temporal patterns. *Hydrol. Earth Syst. Sci.* 22(3): 2041-2056. https://doi.org/10.5194/hess-22-2041-2018.

Hettiarachchi, S., Wasko, C., Sharma, A., 2022a. Do longer dry spells associated with warmer years compound the stress on global water resources? *Earth's Future* 10(2): e2021EF002392. https://doi.org/10.1029/2021EF002392.

Hettiarachchi, S., Wasko, C., Sharma, A., 2022b. Rethinking urban storm water management through resilience–The case for using green infrastructure in our warming world. *Cities* 128: 103789. https://doi.org/10.1016/j.cities.2022.103789.

Hou, X., Guo, H., Wang, F., Li, M., Xue, X., Liu, X., Zeng, S., 2020. Is the sponge city construction sufficiently adaptable for the future stormwater management under climate change? *J. Hydrol.* 588: 125055. https://doi.org/10.1016/j.jhydrol.2020.125055.

Huang, C. L., Hsu, N. S., Liu, H. J., Huang, Y. H., 2018. Optimization of low impact development layout designs for megacity flood mitigation. *J. Hydrol.* 564: 542-558. https://doi.org/10.1016/j.jhydrol.2018.07.044.

Jhong, B.-C., Tung, C.-P., 2018. Evaluating Future Joint Probability of Precipitation Extremes with a Copula-Based Assessing Approach in Climate Change. *Water Resour. Manag.* 32(13): 4253-4274. https://doi.org/10.1007/s11269-018-2045-y.

Karl, T. R., Knight, R. W., 1998. Secular Trends of Precipitation Amount, Frequency, and Intensity in the United States. *Bull. Am. Meteorol. Soc.* 79(2): 231-241. https://dx.doi.org/10.1175/1520-0477(1998)079<0231:stopaf>2.0.co;2.

Klenzendorf, B., Barrett, M., Christman, M., Quigley, M., 2015. Water Quality and Conservation Benefits Achieved via Real Time Control Retrofit of Stormwater Management Facilities near Austin, Texas. StormCon, Austin, TX.

Köppen, W., 1900. Versuch einer Klassifikation der Klimate, Vorzugsweise nach ihren Beziehungen zur Pflanzenwelt [Attempted climate classification in relation to plant distributions]. [In German]. *Geogr. Z.*, 6, 593-611, 657-679.

Leopold, L. B., 1968. Hydrology for urban land planning: A guidebook on the hydrologic effects of urban land use, US Geological Survey.

Louisiana Department of Environmental Quality (LDEQ), 2010. Stormwater BMP Guidance Tool. Compiled by Geosyntec Consultants, New Orleans, LA.

Mahmoud, S. H., Gan, T. Y., 2018. Urbanization and climate change implications in flood risk management: Developing an efficient decision support system for flood susceptibility mapping. *Sci. Total Environ.* 636: 152-167. https://doi.org/10.1016/j.scitotenv.2018.04.282.

Manka, B. N., Hathaway, J. M., Tirpak, R. A., He, Q., Hunt, W. F., 2016. Driving forces of effluent nutrient variability in field scale bioretention. *Ecol. Eng.* 94: 622-628. https://doi.org/10.1016/j.ecoleng.2016.06.024.

Massachusetts Department of Environmental Protection (MassDEP), 2008. Massachusetts Stormwater Handbook Volume 2. Massachusetts Department of Environmental Protection, Boston, MA.

Masson-Delmotte, V., Zhai, P., Pörtner, H.-O., Roberts, D., Skea, J., Shukla, P.R., Pirani, A., Moufouma-Okia, W., Péan, C., Pidcock, R., Connors, S., Matthews, J.B.R., Chen, Y., Zhou, X., Gomis, M.I., Lonnoy, E., Maycock, T., Tignor, M., Waterfield, T., 2018. Global Warming of 1.5°C. An IPCC Special Report on the impacts of global warming of 1.5°C above pre-industrial levels and related global greenhouse gas emission pathways, in the context of strengthening the global response to the threat of climate change, sustainable development, and efforts to eradicate poverty, IPCC.

McGinnis, S., 2018. climod: Bias correction and other tools for climate model output. Version 0.0.1. Accessed March 10, 2021. https://github.com/sethmcg/climod.

McGinnis, S., Nychka, D., Mearns, L. O., 2015. A new distribution mapping technique for climate model bias correction. *Machine learning and data mining approaches to climate science*, Springer: 91-99.

McGinnis, S. A., Mearns, L., 2016. Bias-Correction of Extreme Temperatures and Precipitation in NA-CORDEX Regional Climate Model Output. AGUFM 2016: GC53B-1290.

[dataset] Mearns et al., 2017. The NA-CORDEX dataset, version 1.0. NCAR Climate Data Gateway. Accessed March 2, 2021. https://doi.org/10.5065/D6SJ1JCH.

Miller, R., 1978. The hydraulically effective impervious area of an urban basin, Broward County, Florida. Prepared for the International Symposium on Urban Storm Water Management, Kentucky University, Lexington, July 24-27, 1978.

Milly, P., Betancourt, J., Falkenmark, M., Hirsch, R. M., Kundzewicz, Z. W., Lettenmaier, D. P., Stouffer, R. J., 2008. Stationarity is dead: Whither water management? *Science* 319(5863): 573-574. https://www.science.org/doi/10.1126/science.1151915

Minnesota Stormwater Steering Committee (MSSC), 2006. Minnesota Stormwater Manual. Minnesota Pollution Control Agency, St. Paul, MN.

[dataset] National Oceanic and Atmospheric Administration (NOAA), 2016. National Centers for Environmental Information. Accessed June 1, 2020. https://www.ncdc.noaa.gov/.

[dataset] National Oceanic and Atmospheric Administration (NOAA), 2017. National Weather Service. Accessed January 20, 2021. https://hdsc.nws.noaa.gov/hdsc/pfds/.

North Carolina Department of Environmental Quality (NCDEQ), 2020. NCDEQ Stormwater Design Manual. North Carolina Department of Environmental Quality, Raleigh, NC.

O'Driscoll, M., Clinton, S., Jefferson, A., Manda, A., McMillan, S., 2010. Urbanization Effects on Watershed Hydrology and In-Stream Processes in the Southern United States. *Water* 2(3): 605-648. https://dx.doi.org/10.3390/w2030605.

Olsson, J., Berggren, K., Olofsson, M., Viklander, M., 2009. Applying climate model precipitation scenarios for urban hydrological assessment: A case study in Kalmar City, Sweden. *Atmos. Res.* 92(3): 364-375. https://doi.org/10.1016/j.atmosres.2009.01.015.

Palynchuk, B., Guo, Y., 2008. Threshold analysis of rainstorm depth and duration statistics at Toronto, Canada. *J. Hydrol.* 348(3-4): 535-545. https://doi.org/10.1016/j.jhydrol.2007.10.023.

Persaud, P. P., Akin, A. A., Kerkez, B., McCarthy, D. T., Hathaway, J. M., 2019. Real time control schemes for improving water quality from bioretention cells. *Blue-Green Syst.* 1(1): 55-71. https://doi.org/10.2166/bgs.2019.924.

Pitt, R. E., 1999. Small storm hydrology and why it is important for the design of stormwater control practices. *J. Water Manag. Model.* R204-04.

Pittsburgh Water and Sewer Authority (PWSA), 2022. The City of Pittsburgh Stormwater Design Manual. Pittsburgh Water and Sewer Authority, Pittsburgh, PA.

Prein, A. F., Rasmussen, R. M., Ikeda, K., Liu, C., Clark, M. P., Holland, G. J., 2017. The future intensification of hourly precipitation extremes. *Nat. Clim. Change* 7(1): 48-52. https://doi.org/10.1038/nclimate3168.

Prudhomme, C., Giuntoli, I., Robinson, E. L., Clark, D. B., Arnell, N. W., Dankers, R., Fekete, B. M., Franssen, W., Gerten, D., Gosling, S. N., Hagemann, S., Hannah, D. M., Kim, H., Masaki, Y., Satoh, Y., Stacke, T., Wada, Y., Wisser, D., 2014. Hydrological droughts in the 21st century, hotspots and uncertainties from a global multimodel ensemble experiment. *Proc. Natl. Acad. Sci.* 111(9): 3262-3267. https://doi.org/10.1073/pnas.1222473110.

Pryor, S. C., Howe, J. A., Kunkel, K. E., 2009. How spatially coherent and statistically robust are temporal changes in extreme precipitation in the contiguous USA? *Int. J. Climatol.* 29(1): 31-45. https://dx.doi.org/10.1002/joc.1696.

R Core Team, 2020. R: A language and environment for statistical computing. R Foundation for Statistical Computing, Vienna, Austria. Accessed March 10, 2020. http://www.r-project.org/index.html.

Rosenberg, E. A., Keys, P. W., Booth, D. B., Hartley, D., Burkey, J., Steinemann, A. C., Lettenmaier, D. P., 2010. Precipitation extremes and the impacts of climate change on stormwater infrastructure in Washington State. *Clim. Change* 102(1): 319-349. https://doi.org/10.1007/s10584-010-9847-0.

Rossman, L., 2015. Storm Water Management Model User's Manual Version 5.1—Manual. US EPA Office of Research and Development, EPA: Washington, DC, USA.

Roy, A. H., Freeman, M. C., Freeman, B. J., Wenger, S. J., Ensign, W. E., Meyer, J. L., 2005. Investigating hydrologic alteration as a mechanism of fish assemblage shifts in urbanizing streams. *J. N. Am. Benthol. Soc.* 24(3): 656-678. https://doi.org/10.1899/04-022.1.

San Antonio River Authority (SARA), 2019. San Antonio River Basin Low Impact Development Technical Design Guidance Manual, v2. San Antonio River Authority, San Antonio, TX.

Sarkar, S., Butcher, J. B., Johnson, T. E., Clark, C. M., 2018. Simulated sensitivity of urban green infrastructure practices to climate change. *Earth Interact.* 22(13): 1-37. https://doi.org/10.1175/EI-D-17-0015.1.

Shen, P., Deletic, A., Bratieres, K., McCarthy, D. T., 2020. Real time control of biofilters delivers stormwater suitable for harvesting and reuse. *Water Res.* 169: 115257. https://doi.org/10.1016/j.watres.2019.115257.

Shuster, W. D., Bonta, J., Thurston, H., Warnemuende, E., Smith, D. R., 2005. Impacts of impervious surface on watershed hydrology: A review. *Urban Water J.* 2(4): 263-275. https://doi.org/10.1080/15730620500386529.

Stephens, G. L., L'Ecuyer, T., Forbes, R., Gettelmen, A., Golaz, J. C., Bodas- Salcedo, A., Suzuki, K., Gabriel, P., Haynes, J., 2010. Dreary state of precipitation in global models. *J. Geophys. Res. Atmos.* 115(D24). https://doi.org/10.1029/2010JD014532.

Strauss, F., Formayer, H., Schmid, E., 2013. High resolution climate data for Austria in the period 2008–2040 from a statistical climate change model. *Int. J. Climatol*. 33(2): 430-443. https://doi.org/10.1002/joc.3434.

Tennessee Department of Environment and Conservation (TDEC), 2014. Tennessee Permanent Stormwater Management and Design Guidance Manual. Tennessee Department of Environment and Conservation, Division of Water Resources, Nashville, TN.

Tirpak, A., Hathaway, J. M., Khojandi, A., Weathers, M., Epps, T. H., 2021. Building Resiliency to Climate Change Uncertainty through Bioretention Design Modifications. *J. Environ. Manage.* 287: 112300. https://doi.org/10.1016/j.jenvman.2021.112300.

van Vuuren, D. P., Edmonds, J., Kainuma, M., Riahi, K., Thomson, A., Hibbard, K., Hurtt, G. C., Kram, T., Krey, V., Lamarque, J. F., Masui, T., Meinshausen, M., Nakicenovic, N., Smith, S. J., Rose, S. K., 2011. The representative concentration pathways: an overview. *Clim. Change*. 109(1): 5-31. https://doi.org/10.1007/s10584-011-0148-z.

Vijayaraghavan, K., Biswal, B. K., Adam, M. G., Soh, S. H., Tsen-Tieng, D. L., Davis, A. P., Chew, S. H., Tan, P. Y., Babovic, V., Balasubramanian, R., 2021. Bioretention systems for stormwater management: Recent advances and future prospects. *J. Environ. Manage.* 292: 112766. https://doi.org/10.1016/j.jenvman.2021.112766.

Walsh, C. J., Roy, A. H., Feminella, J. W., Cottingham, P. D., Groffman, P. M., Morgan, R. P., 2005. The urban stream syndrome: current knowledge and the search for a cure. *J. N. Am. Benthol. Soc.* 24(3): 706-723. https://dx.doi.org/10.1899/04-028.1.

Wang, M., Zhang, D. Q., Su, J., Dong, J. W., Tan, S. K., 2018. Assessing hydrological effects and performance of low impact development practices based on future scenarios modeling. *J. Clean. Prod.* 179: 12-23. https://doi.org/10.1016/j.jclepro.2018.01.096.

Wang, M., Zhang, D., Cheng, Y., Tan, S. K., 2019a. Assessing performance of porous pavements and bioretention cells for stormwater management in response to probable climatic changes. *J. Environ. Manage.*, 243: 157-167. https://doi.org/10.1016/j.jenvman.2019.05.012.

Wang, M., Zhang, D., Lou, S., Hou, Q., Liu, Y., Cheng, Y., Qi, J., Tan, S. K., 2019b. Assessing hydrological effects of bioretention cells for urban stormwater runoff in response to climatic changes. *Water* 11(5): 997. https://doi.org/10.3390/w11050997.

Wasko, C., Sharma, A., 2015. Steeper temporal distribution of rain intensity at higher temperatures within Australian storms. *Nat. Geosci.* 8(7): 527-529. https://doi.org/10.1038/ngeo2456.

Winston, R. J., 2016. Resilience of Green Infrastructure under Extreme Conditions. Doctoral dissertation, Raleigh, NC: North Carolina State Univ.

Winston, R. J., Dorsey, J. D., Hunt, W. F., 2016. Quantifying volume reduction and peak flow mitigation for three bioretention cells in clay soils in northeast Ohio. *Sci. Total Environ.* 553: 83-95. https://doi.org/10.1016/j.scitotenv.2016.02.081.

Yang, L., Ni, G., Tian, F., Niyogi, D., 2021. Urbanization exacerbated rainfall over European suburbs under a warming climate. *Geophys. Res. Lett.* 48(21): e2021GL095987. https://doi.org/10.1029/2021GL095987.

Zhang, W., Villarini, G., Vecchi, G. A., Smith, J. A., 2018. Urbanization exacerbated the rainfall and flooding caused by hurricane Harvey in Houston. *Nature* 563(7731): 384-388. https://doi.org/10.1038/s41586-018-0676-z.

Zhang, K., Manuelpillai, D., Raut, B., Deletic, A., Bach, P. M., 2019. Evaluating the reliability of stormwater treatment systems under various future climate conditions. *J. Hydrol.* 568: 57-66. https://doi.org/10.1016/j.jhydrol.2018.10.056.